

C1-Interpolation for Vector Field Topology Visualization

Gerik Scheuermann

Xavier Tricoche

Hans Hagen

University of Kaiserslautern

Department of Computer Science, Computer Graphics & CAGD

P.O. Box 3049, D-67653 Kaiserslautern

Germany

E-mail: {scheuer|tricoche|hagen}@informatik.uni-kl.de

Abstract

An application of C^1 scalar interpolation for 2D vector field topology visualization is presented. Powell-Sabin and Nielson interpolants are considered which both make use of Nielson's Minimum Norm Network for the precomputation of the derivatives in our implementation. A comparison of their results to the commonly used linear interpolant underlines their significant improvement of singularity location and topological skeleton depiction. Evaluation is based upon the processing of polynomial vector fields with known topology containing higher order singularities.

Keywords: vector field visualization, topology, critical point theory, C^1 -interpolation

1 Introduction

Vector field visualization is an issue of major interest in many scientific and engineering areas. As a matter of fact, vector fields offer a qualitative and quantitative description of numerous natural phenomena. In physics, they play a fundamental role in fluid dynamics, solid mechanics, electricity or magnetism, among others. They are also impossible to circumvent for engineers that massively make use of them in disciplines like computational fluid dynamics (CFD), finite element analysis (FEA) and computer aided design (CAD). Typically, measurements or numerical simulations provide analysts with increasingly large vector data sets. This raw data must next be properly conveyed for interpretation. The aim of vector field visualization is to offer a convenient way to extract this information. But to be of any interest, the display has to focus efficiently on the most meaningful aspects of the data to avoid confusing the results.

Among the existing techniques in this sphere, topology-based methods have proved to be very successful in enabling a good insight into the qualitative nature of the vector field while reducing the size of the data. Their basic principle is to locate and classify the critical points (i.e. zeros) of the field and to draw a small number of streamlines connecting them, separating the field into regions of equal qualitative behavior.

As a preliminary step of the topology extraction, one has to work out the interpolation of the given discrete data. A commonly used solution is the computation of a linear interpolant over each cell of the triangulated (unstructured) point set. One problematic aspect of this method is that the linear interpolant is inaccurate when being confronted with several very close critical points or with higher order singularities: zeros are moved or split up and the global topology is thus likely to be altered. Furthermore, one gets piecewise constant differential fields (e.g. divergence, curl) that cannot be meaningfully compared to experimental measurements or simulations. Consequently, consistency is lost between the vector field and its associated differential fields.

This paper presents two higher order interpolation schemes applied to vector field topology visualization. It is shown that the

topology is in both cases better reproduced than by piecewise linear interpolation. Furthermore, unlike the latter, C^1 -interpolation successfully attacks the problem of additional critical points. At last, the resulting topological skeletons appear more reliable and easier to analyze.

The structure of the paper is as follows. We start with a review of the literature dealing with vector field topology detection and higher order methods designed to improve the accuracy of the traditional linear schemes. C^1 -scalar interpolation is then discussed where we use Nielson's Minimum Norm Network to obtain derivative information. We present two interpolation schemes, namely Powell-Sabin method and Nielson method that achieve a C^1 -continuity over the triangulation. In section 4, we repeat some basic definitions of vector field topology. Implementation aspects are discussed in section 5. Finally, results are shown in the last part, which consists of a comparison of the topological skeletons obtained with both C^1 -interpolants and the classical linear interpolation.

2 Related Work

Topology-based methods were introduced in vector field visualization by Helman and Hesselink about ten years ago (see [Hel89], [Hel91]). Their basic principle stems from critical point theory: One focuses on few features of the field, namely its critical points (where the field is zero) and the streamlines connecting them (the so-called *separatrices*) to get a domain decomposition into subregions that are all topologically equivalent to a uniform flow. Helman and Hesselink restricted their study to a first order approximation that is, by only considering the jacobian matrix at critical points to infer the local aspect of the field around them. This work gave rise to several extensions: Globus et al. ([Glo91]) developed a visualization environment called *FAST* in which they extract and visualize topology of 3D vector fields; Bajaj et al. ([Baj98]) applied such a topology-based method to scalar field visualization; Nielson et al. (see [Nie97]) applied several explicit methods to the computation of tangential curves and topological graphs in the case of 2D vector fields, linearly interpolated over a triangulation.

Most methods assume that the initial scattered vector data have been reconstructed into a continuous field by a piecewise linear interpolation over a beforehand computed triangulation of the given sample points. It explains the first order restriction of former topology-based methods. Nevertheless, the linear interpolation of a vector field can yield a large number of critical points. In particular, two neighboring triangles may contain critical points of different kinds (namely of indices +1 and -1, see section 4). Such effects are not desirable for they artificially increase the complexity of the topology. To address this problem, Scheuermann and Hagen (see [Sch98b]) proposed a data dependent triangulation based upon the fact that if two neighboring triangles both contain a zero, the two new triangles obtained by swapping their common edge do not. One achieves in that way a significant reduction of the number of critical

points which clarifies the resulting depiction of the field.

Futhermore, the linear interpolant which is clearly unable to convey higher-order singularities, introduces topological artefacts such as splitting into several simple critical points (lying in different triangles) of higher order zeros. To deal with this deficiency, Scheuermann et al. (see [Sch98c]) introduced higher order polynomials to process the area located around such critical points: starting with a linear interpolation over a triangulation of the points, they next look for neighboring triangles containing several zeros and then compute inside them a polynomial approximation of the data. The choice of these polynomials is motivated by Clifford analysis, mathematical background of their study. Problems remain when connecting the linear interpolated triangles with the "higher order" cells for, in the latter, the data are not interpolated.

There has been also some work using higher order derivatives: last year, Roth and Peikert (see [Rot98]) showed the use of higher order derivatives for finding bent vortices.

3 C1-Interpolation

C^1 -interpolation over triangles is an issue that has been widely studied for about 30 years. As a consequence, there are many existing interpolants in this field. Nevertheless, in our case, we are interested in the topology (see 4) extraction of the resulting interpolated field. That is, we have to concentrate on schemes that are computation-efficient as well as able to result in a meaningful topology. These considerations led us to restrict our implementation to only two methods: Nielson's C^1 -interpolant ([Nie83]) and the Powell-Sabin scheme ([Pow77]).

As a preliminary step, both methods require derivative information at each vertex of the scattered data. As we said in the introduction, in a first step we have computed an (optimal) Delaunay triangulation and are thus in a position to treat the data globally for this goal. The derivatives are then estimated using Nielson's Minimum Norm Network.

3.1 Derivatives Computation: Nielson's Minimum Norm Network

Let us introduce some convenient notations: We are given a set of N points V_1, \dots, V_N . T_{ijk} denotes the triangle with vertices V_i, V_j, V_k , e_{ij} represents the edge linking V_i to V_j and N_e is a list of the indices representing the edges of the triangulation. The curve network is thus defined over $E = \cup_{ij \in N_e} e_{ij}$. We also define the following directional derivative:

The derivative along an edge is given by

$$\frac{\partial F}{\partial e_{ij}} = \frac{(x_j - x_i)}{\|e_{ij}\|} \frac{\partial F}{\partial x} + \frac{(y_j - y_i)}{\|e_{ij}\|} \frac{\partial F}{\partial y}$$

where $\|e_{ij}\|$ is the length of e_{ij} .

Now we consider the problem of finding an interpolating curve network which minimizes, for $F \in C[E] = \{F : F \text{ is the restriction to } E \text{ of some } C^1 \text{ function defined on } D, \text{ union of all triangles}\}$:

$$\sigma(F) = \sum_{ij \in N_e} \int_{e_{ij}} \left[\frac{\partial^2 F}{\partial e_{ij}^2} \right]^2 ds_{ij}$$

where ds_{ij} represents the element of arc length on the curve consisting of the line segment e_{ij} . We have then the following result: Let $S \in C[F]$ be the unique piecewise cubic network, with the properties that $S(V_i) = z_i$, $i = 1, \dots, N$ and

$$\bullet \sum_{ij \in N_i} \frac{(x_j - x_i)}{\|e_{ij}\|^3} [(x_j - x_i)S_x(V_i) + (y_j - y_i)S_y(V_i)$$

$$+ \frac{1}{2}(x_j - x_i)S_x(V_j) + \frac{1}{2}(y_j - y_i)S_y(V_j) - \frac{3}{2}(z_j - z_i)] = 0$$

$$\bullet \sum_{ij \in N_i} \frac{(y_j - y_i)}{\|e_{ij}\|^3} [(x_j - x_i)S_x(V_i) + (y_j - y_i)S_y(V_i)$$

$$+ \frac{1}{2}(x_j - x_i)S_x(V_j) + \frac{1}{2}(y_j - y_i)S_y(V_j) - \frac{3}{2}(z_j - z_i)] = 0$$

where $N_i = \{ij : e_{ij} \text{ is the edge of the triangulation with the endpoint } V_i(x_i, y_i)\}$, and

$$S_x(V_i) = \frac{\partial S}{\partial x}(V_i).$$

Then, among all functions $F \in C[E]$, $F(V_i) = z_i$, $i = 1, \dots, N$, the function S uniquely minimizes $\sigma(F)$.

Solving this linear system in $S_x(V_i)$ and $S_y(V_i)$, $i = 1, \dots, N$, one is able to build a cubic polynomial curve on each edge e_{ij} by Hermite interpolation.

3.2 Interpolation

Once the derivatives have been estimated at each vertex of the scattered data, an interpolation must be processed over each triangle which ensures C^1 continuity at the edges of the triangulation. We start with a brief description of the Powell-Sabin method which does not fulfil the requirements of the Minimum Norm Network (for its restriction on the edges is not a cubic polynomial) but enables an analytic search of its roots (see 4).

3.2.1 Powell-Sabin Interpolant

This method is based on the following remark: a biquadratic polynomial is unable to fit both values and derivatives at each vertex of a triangle because it offers only 6 degrees of freedom and there are 9 interpolation conditions to fulfil. So we need to increase the degrees of freedom. This may be achieved thanks to a subdivision of each triangle into 6 subtriangles (see Figure 1). Starting with a bi-

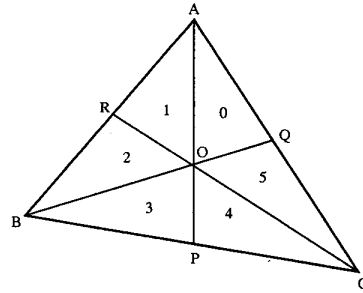


Figure 1: Division of ABC into 6 triangles

quadratic polynomial defined over triangle OAQ, say $q_0(x, y)$, one then adds a correction term each time one crosses an internal edge, moving in a clockwise direction around O. The only quadratic solutions for this correction term, that ensure the required C^1 continuity through the edge have the form:

$$\lambda_i(l_i x + m_i y + n_i)^2$$

where $(l_i x + m_i y + n_i)$ is the cartesian equation of the i -th crossed edge and λ_i is the parameter to adjust.

Ensuring the interpolation conditions for values and derivatives and forcing

$$\sum_{i=0}^5 \lambda_i (l_i x + m_i y + n_i)^2 \equiv 0$$

one gets a non singular linear system with 12 (not independent) variables. By solving it, one obtains the desired piecewise bi-quadratic C^1 interpolant. (see [Pow77]).

3.2.2 Nielson's Blending Method

The second C^1 -continuous method is Nielson's C^1 Side-Vertex blending method (see [Nie83]). This scheme profits more from the Minimum Norm Network we introduced previously for it respects the cubic curves built on the edges of the triangulation. However, since it consists of a rational function with quintic numerator, its zeros may not be found analytically (see 5.2.1).

To extend the scalar values defined on the edges to the whole domain, Nielson proposes the following formula:

For any point (x, y) with barycentric coordinates b_i, b_j, b_k in a triangle with vertices V_i, V_j, V_k , one sets:

$$C_{\Delta}[F](x, y) =$$

$$\sum_{(i,j,k) \in I} \left\{ F(V_i) [b_i^2 (3 - 2b_i) + 6\omega b_i (b_k \alpha_{ij} + b_j \alpha_{ik})] \right. \\ \left. + F'_{ki}(V_i) [b_i^2 b_k + \omega b_i (3b_k \alpha_{ij} + b_j - b_k)] \right. \\ \left. + F'_{ji}(V_i) [b_i^2 b_j + \omega b_i (3b_j \alpha_{ik} + b_k - b_j)] \right\}$$

where

$$F'_{ki}(V_i) = (x_k - x_i)F_x(V_i) + (y_k - y_i)F_y(V_i), \\ F'_{ji}(V_i) = (x_j - x_i)F_x(V_i) + (y_j - y_i)F_y(V_i),$$

$$\omega = \frac{b_i b_j b_k}{b_i b_j + b_i b_k + b_j b_k}, \quad I = \{(i, j, k), (j, k, i), (k, i, j)\},$$

and

$$\alpha_{ij} = \frac{\|e_{jk}\|^2 + \|e_{ik}\|^2 - \|e_{ij}\|^2}{2\|e_{ik}\|^2}$$

This defines a 9-parameter, C^1 interpolant.

4 Vector Field Topology

As said previously, vector field topology consists of the association of critical points with some particular streamlines. In this work, we adopted the concept of topological skeleton proposed by Helman and Hesselink (see [Hel91]).

Let us recall that we consider the eigenvalues of the jacobian matrix (restricting our analysis to a linear approximation):

$$\frac{\partial(v_x, v_y)}{\partial(x, y)} \Big|_{(x_0, y_0)} = \begin{pmatrix} \frac{\partial v_x}{\partial x} & \frac{\partial v_x}{\partial y} \\ \frac{\partial v_y}{\partial x} & \frac{\partial v_y}{\partial y} \end{pmatrix} \Big|_{(x_0, y_0)}$$

Depending on their sign and on their imaginary part, one gets 6 possible configurations for the vector field around a singular point (see Figure 2). To describe the qualitative nature of a critical point, one can also use its index:

Let z be an isolated zero of the vector field $v : D \rightarrow \mathbb{R}^2$. Then there is a neighborhood U of z containing only one critical point. Let $U' = U - \{z\}$ and $D_\varepsilon(z) \subset U$ be a closed disc around z of radius ε . Let $\gamma_\varepsilon : S^1 \rightarrow S_\varepsilon \subset U'$ be the boundary curve of

$D_\varepsilon(z)$. We define the index of the critical point z of the vector field v as:

$$\text{ind}_z v = \lim_{\varepsilon \rightarrow 0} \frac{1}{2\pi} \oint_{\gamma_\varepsilon} d\phi$$

where ϕ is the angle coordinate of the vector field, namely

$$d\phi = d \arctan \frac{v_y}{v_x} = \frac{v_y dv_x - v_x dv_y}{v_x^2 + v_y^2}$$

The index measures the number of rotations of the flow around a critical point.

Notice that for the special case of singularities of first order, the possible values of the index are +1 and -1.

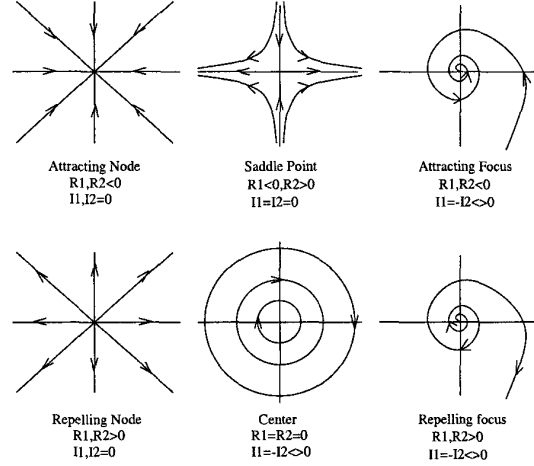


Figure 2: possible configurations of 1st-order singular points. R_1, R_2 denote the real parts of the eigenvalues and I_1, I_2 their imaginary parts

5 Locating Critical Points

The topology extraction of a vector field starts with the location of its singular points. In this section we explain how we have detected them for both interpolants.

5.1 Powell-Sabin Case

In the presentation of this method, we underlined the fact that it is possible to determine algebraically the zeros of a biquadratic polynomial. The method is as follows.

Let

$$P(x, y) = a_0 + a_1 x + a_2 y + a_3 xy + a_4 x^2 + a_5 y^2 \\ Q(x, y) = b_0 + b_1 x + b_2 y + b_3 xy + b_4 x^2 + b_5 y^2$$

be two quadratic polynomials which common roots have to be found. We may consider each bivariate polynomial as a polynomial in the y variable (i.e. x becomes a parameter):

$$P_x(y) = (a_0 + a_1 x + a_4 x^2) + (a_2 + a_3 x)y + a_5 y^2 \\ := \alpha_0(x) + \alpha_1(x)y + \alpha_2 y^2 \\ Q_x(y) = (b_0 + b_1 x + b_4 x^2) + (b_2 + b_3 x)y + b_5 y^2 \\ := \beta_0(x) + \beta_1(x)y + \beta_2 y^2$$

We next introduce the so-called *resultant* of the system, defined by:

$$R(P_x, Q_x) = \begin{vmatrix} \alpha_0(x) & \alpha_1(x) & \alpha_2 & 0 \\ 0 & \alpha_0(x) & \alpha_1(x) & \alpha_2 \\ \beta_0(x) & \beta_1(x) & \beta_2 & 0 \\ 0 & \beta_0(x) & \beta_1(x) & \beta_2 \end{vmatrix}$$

with the property that $R(P_x, Q_x) = 0$ if and only if P_x and Q_x have a root in common. Now $R(P_x, Q_x)$ is a 4th-order polynomial in the x variable which roots may be found thanks to classical methods. The found x values must now be replaced in either the equation of $P_x(y)$ or $Q_x(y)$ to get a quadratic polynomial which roots are the zeros of the system.

In our special case, we obviously have to check if the roots lie inside the subtriangle where the considered biquadratic polynomial describes the vector field.

5.2 Nielson Case

To compute the position of the zeros for Nielson bi-rational interpolant, one has to solve a system of two equations of fifth order. Since this is a very difficult algebraic task, we use numerical algorithms. Unfortunately, the existing algorithms need to be provided with a “good” initial guess to start their search and we can not infer easily, a priori, an approximate location of the singular points in the interpolated field. These remarks led us to adopt the following heuristic: as a first step, we find out which triangles may potentially contain one or more zeros (actually, one could find up to 25 zeros for such a polynomial system, even if this is practically very unlikely to occur); then we divide each so-called “candidate triangle” in 25 subtriangles, in which we process the same analysis; in the last step we use the barycenter of each candidate subtriangle as first guess for a numerical search, assuming that only one zero, at the most, is in a subtriangle. Let us detail these topics.

5.2.1 Finding Candidate Triangles

The aim of this procedure is to avoid numerical searches in vain. To keep efficiency in our processing, we have to take away the triangles that can not contain any critical point. But to be of any practical use, this dichotomy has to be fast, so we focus on the control polygons of the cubic polynomial defined along the edges of each triangle. The reason is that when we build Nielson’s interpolant over each triangle, we compute a blending of the splines on the edges so that a kind of energy criterion is minimized (see 3.2.2). Consequently, if no spline on the border crosses the X-Y plane, we assume that also the interpolant over the triangle does not which has been confirmed by our numerical tests. So we have to check for each dimension, if a spline has a root. To speed up that process, we approximate the behaviour of the spline by its control polygon, easily defined by both value and derivative of the field at both vertices of the edge. Five¹ generic configurations may occur (see Figure 3), from which four may lead to a zero (namely, in case 1, one has no zero, whereas in cases 2 and 3, there is exactly one zero, and in cases 4 and 5 one has either 2 or no zeros). If we get such “zero”-configurations for both dimensions then the triangle is marked as “candidate” and will be processed further.

This kind of sign test is similar to the scheme proposed by Asimov et al. to find candidate cells in the case of a bilinear interpolant ([Tut92]).

¹a sixth configuration is theoretically possible which has 3 roots but this situation does not occur in our case for the splines on the edges minimize the pseudonorm introduced in 3.1

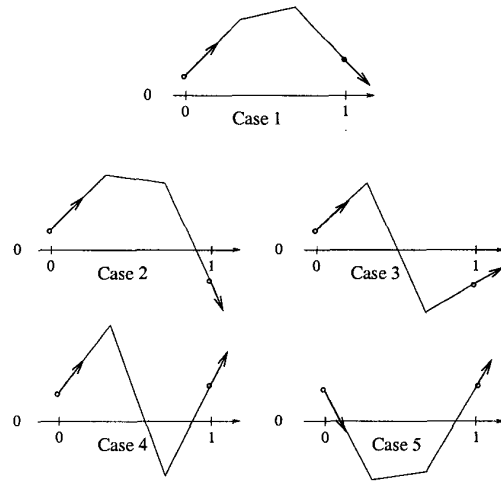


Figure 3: generic configurations of the Bézier control polygon for a cubic polynomial

5.2.2 Processing the Subtriangles

Each candidate triangle is divided into 25 subtriangles assuming only up to one simple zero in each subtriangle. This is motivated by the fact that our birational interpolant may have up to 25 zeros on the one hand and that 2 zeros should not be too close together on the other hand, for this would mean an oscillation of the interpolant, quite incompatible with its pseudo-energy minimization property. Then we compute the value of the index (see 4) of each subtriangle: a value +1 or -1 shows the presence of a critical point (see Figure 4).

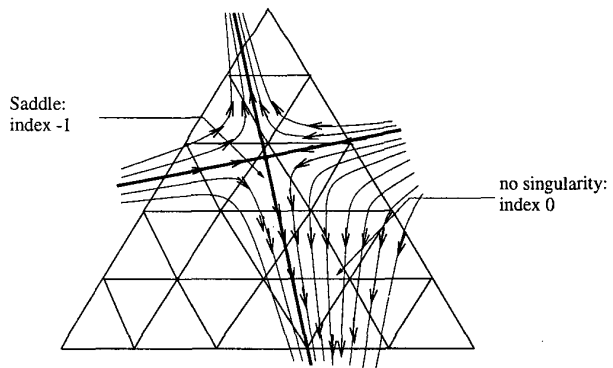


Figure 4: index of subtriangles

Remark that the index method was not used for the “big” triangles because one may get several critical points in the same triangle, which can lead to a 0 index computed on its border, while it actually contains singularities (for example, the problem occurs when a saddle and an attracting focus lie in the same triangle: the sum of their indices is $-1 + 1 = 0$ and one misses two critical points as in Figure 5).

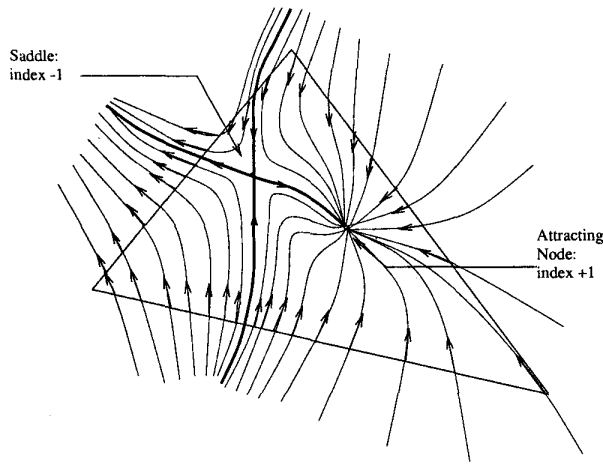


Figure 5: triangle with index 0 containing a saddle and an attracting focus

5.2.3 Numerical Search

The former steps intended to provide a “good” first guess for a numerical search. We have eliminated all the triangles that do not contain a critical point and determined (small) subtriangles that actually contain a single zero. We can now take the barycenter of each selected subtriangle as first guess. For the numerical search, the Newton-Raphson algorithm is applied, which works satisfactorily for our needs.

6 Results

6.1 Test Data

The test of our interpolation schemes requires a precise description of the topology of the underlying vector field. A suitable solution is the use of vector fields given by a single formula with known topology. Furthermore, to prove the accuracy of our algorithm, we must be able to design topological aspects of the field, like close critical points, higher order critical points,...

The only vector fields that are usually known topologically are linear fields or some special cases with strong restrictions. In a previous paper, we proved a theorem that enables the design of polynomial vector fields with higher order singularities. We bring back here the main results (see [Sch98a]).

Let (e_1, e_2) be the canonical basis of R^2 and let

$$v(r) = \operatorname{Re}(az + b\bar{z} + c)e_1 - \operatorname{Im}(az + b\bar{z} + c)e_2$$

be a linear vector field with $r = xe_1 + ye_2$, $z = x + iy$, $a, b, c \in C$. For $|a| \neq |b|$, it has a unique zero at $\operatorname{Re}(z_0)e_1 + \operatorname{Im}(z_0)e_2 \in R^2$. For $|a| > |b|$, v has a saddle with index -1, and for $|a| < |b|$, it has one critical point with index 1. The special types in this case are shown in the following list:

1. $\operatorname{Re}(b) = 0 \Leftrightarrow$ circle at z_0 .
2. $\operatorname{Re}(b) \neq 0, |a| > |\operatorname{Im}(b)| \Leftrightarrow$ node at z_0 .
3. $\operatorname{Re}(b) \neq 0, |a| < |\operatorname{Im}(b)| \Leftrightarrow$ spiral at z_0 .
4. $\operatorname{Re}(b) \neq 0, |a| = |\operatorname{Im}(b)| \Leftrightarrow$ focus at z_0 .

In cases 2)-4) one has a sink for $\operatorname{Re}(b) < 0$ and a source for $\operatorname{Re}(b) > 0$. For $|a| = |b|$ one gets a whole line of zeros.

For our needs, we use the following theorem:

Let $v : R^2 \rightarrow R^2$ be the vector field

$$v(r) = \operatorname{Re}(E(z, \bar{z}))e_1 - \operatorname{Im}(E(z, \bar{z}))e_2$$

with

$$E(z, \bar{z}) = \prod_{k=1}^n (a_k z + b_k \bar{z} + c_k), \quad |a_k| \neq |b_k|,$$

and let z_k be the unique zero of $a_k z + b_k \bar{z} + c_k$. Then v has zeros at z_j , $j = 1, \dots, n$, and the index of v at z_j is the sum of the indices of $\operatorname{Re}(a_k z + b_k \bar{z} + c_k)e_1 - \operatorname{Im}(a_k z + b_k \bar{z} + c_k)e_2$ at z_j .

(That is, we only use linear factors).

Remember that a critical point with index -1 is a saddle point, whereas a critical point with index +1 may be a circle, a node, a spiral or a focus. Practically, it means that when we design our vector fields we are able to locate the saddle points and the critical points of index +1 (the precise nature can not be predefined) as well as to define critical points of higher order by giving $a_k z + b_k \bar{z} + c_k$ a multiplicity higher than 1 in the expression for $E(z, \bar{z})$.

6.2 Examples

The presentation of our results is based upon the comparison of the C^1 -methods to a piecewise linear interpolation of the same data. For each case, the exact topology is used as reference.

6.2.1 First Example

In the first example, we use several simple critical points and one of higher order. The definition of this field is:

Let $D = [-1, 1] \times [-1, 1]$

$$\begin{aligned} v : D &\rightarrow R^2 \\ r &\mapsto (z - (0.74 + 0.35i))(z - (0.68 - 0.59i)) \\ &\quad (z - (-0.11 - 0.72i)(\bar{z} - \frac{-0.58 - 0.64i}{-0.58 - 0.64i})) \\ &\quad (\bar{z} - \frac{0.51 + 0.27i}{0.51 + 0.27i})(\bar{z} - \frac{-0.12 - 0.84i}{-0.12 - 0.84i})^2 e_1 \end{aligned}$$

(An overview of the topology is shown in Figure 6).

Starting with 500 samples, one gets the topological skeleton of Figure 7 in the linear case. The resulting topology is erroneous: singularities are missed which entails the deformation or disappearance of separatrices. Globally, this depiction of the field should be considered as totally unsatisfying.

Nielson C^1 -interpolant produces the result shown in Figure 8. In this case, the global aspect of the topology has been respected. The only topology deformation occurs at the location of the higher order singularity: it has been split up in attracting and repelling foci. With the same points sample one achieves the topology of Figure 9 by applying Powell-Sabin's method. No significant difference appears here, compared to Nielson's method.

By doubling the number of sample points, one gets for all the interpolants a globally satisfying depiction of the topological skeleton. Nevertheless, the area located around the higher order singularity remains problematic in the linear case as shown in the enlargement proposed in Figure 10. That is, although one could expect an improvement of the topology approximation with more

points, as far as the higher order singularity is concerned the results are worse: the whole aspect of the field in this area has been deformed and the presence of an higher order singularity is impossible to guess. Nielson's method offers in this case the same kind of result as for 500 points. However the two foci have become closer which represents an improvement of the higher order singularity approximation. Otherwise, in this case, the Powell-Sabin interpolant confuses the topology depiction by introducing two additional singularities that have no meaningful impact on the global aspect of the topological skeleton (see Figure 11).

6.2.2 Second Example

The second example is defined by the following expression:

$$\text{Let } D = [-1, 1] \times [-1, 1]$$

$$\begin{aligned} v : D &\rightarrow \mathbb{R}^2 \\ r &\mapsto (z - 0.5i)(z - (0.001 + 0.501i)) \\ &\quad (\bar{z} - \overline{-0.5i})^2 e_1 \end{aligned}$$

that is, one has to face two topological difficulties (see Figure 12): two very close saddle points on one hand and a singularity of higher order (namely of index + 2) on the other hand. Starting with a sample of 500 vectors, one has the picture proposed in Figure 13 in the linear case. The most problematic aspect of this field approximation takes place at the second order singularity: it is replaced by 4 first order singularities (namely one saddle and 3 foci) and consequently the original topology is lost locally. Furthermore the two close saddle points have been taken away from another.

Considering Nielson's scheme, the results are shown in Figure 14. Because the two saddles have been maintained very close to each other and the two foci resulting from split of the higher order singularity lie in the same triangle, this topology approximation should be regarded as very satisfying and does not require more data points. The same remark applies to Powell-Sabin interpolant as one can see in Figure 15. If one tries to improve the topology depiction in the linear case by increasing the number of sample points one has to face on the contrary a deterioration of the interpolant performance as already observed with the former example. Figure 16 demonstrates this effect (note that the coarse aspect of the streamlines is due to the enlargement since we have focused on an area that is a factor of 4000 smaller as the original one). Some artefacts also occur in the area located around the saddles as shown in Figure 17.

7 Conclusion

A piecewise linear interpolation of scattered vector data is not an accurate way of reproducing the inner structure of the original vector field in difficult cases. Furthermore, when the topology is unknown a priori, it introduces additional singularities that confuse the results and inconvenience the interpretation.

By using two C^1 interpolation methods, we have arrived at a clearly improved approximation of the original field with the same initial information. Close singularities as well as critical points of higher order are that way better conveyed by both schemes that always keep close to the expected topological skeleton.

Nevertheless we should underline that Nielson's interpolant, thanks to its respect of the precomputed minimum norm network, produces thoughtlessly better results. So in our opinion, it comes out to be the right choice for C^1 -interpolation for the purpose of vector field topology visualization.

Acknowledgements

This research was partly made possible by financial support by the Conseil Général de l'Isère (France). The second author received a

"bourse de projet a l'étranger" during his stay at the university of Kaiserslautern from March 98 to June 98.

References

- [Baj98] Bajaj C.L., Pascucci V., Schikore D.R., *Visualization of Scalar Topology for Structural Enhancement*. Proc. Visualization'98, IEEE Computer Society Press, 1998, pp. 51-58.
- [Glo91] Globus A., Levit C., Lasinski T., *A Tool for Visualizing the Topology of Three-Dimensional Vector Fields*. Proc. Visualization'91, IEEE Computer Society Press, 1991, pp. 17-24.
- [Hel89] Helman J.L., Hesselink L., *Representation and Display of Vector Field Topology in Fluid Flow Data Sets*. IEEE Computer, Aug. 1989, pp. 27-36.
- [Hel91] Helman J.L., Hesselink L., *Visualizing Vector Field Topology in Fluid Flows*. IEEE Computer Graphics and Applications, Vol. 11(3), 1991, pp. 36-46.
- [Nie79] Nielson G.M., *The Side-Vertex Method for Interpolation in Triangles*. Journal of Approximation Theory, Vol. 25, 1979, pp. 318-336.
- [Nie83] Nielson G.M., *A Method for Interpolating Scattered Data Based Upon a Minimum Norm Network*. Mathematics of Computation, Vol. 40, 1983, pp. 253-271.
- [Nie97] Nielson G.M., *Tools for Computing Tangent Curves and Topological Graphs for Visualizing Piecewise Linearly Varying Vector Fields over Triangulated Domains*. In Scientific Visualization, G.M. Nielson, H. Hagen, H. Müller. (eds.), IEEE Computer Society, 1997, pp. 527-562.
- [Pow77] Powell M.J.D, Sabin M.A., *Piecewise Quadratic Approximations on Triangles*. ACM Transactions on Mathematical Software, Vol. 3, No. 4, pp. 316-325, 1977.
- [Rot98] Roth M., Peikert R., *A Higher-Order Method For Finding Vortex Core Lines*. Proc. Visualization '98, IEEE Computer Society, 1998, pp. 143-150.
- [Sch98a] Scheuermann G., Hagen H., Krüger H., *An Interesting Class of Polynomial Vector Fields*. In Mathematical Methods for Curves and Surfaces II, Morton Daehlen, Tom Lyche, Larry L. Schumaker (eds.), Vanderbilt University Press, Nashville, 1998, pp. 429-436.
- [Sch98b] Scheuermann G., Hagen H., *A Data Dependent Triangulation of Vector Fields*. Proc. of Computer Graphics International 1998, Franz-Erich Wolter, Nicholas M. Patrikalakis (eds.), IEEE Computer Society Press, 1998, pp. 96-102.
- [Sch98c] Scheuermann G., Krüger H., Menzel M., Rockwood A.P., *Visualizing Non-Linear Vector Field Topology*. IEEE Transactions On Visualization & Computer Graphics, Vol. 4(2), 1998, pp. 109-116.
- [Tut92] Post F., Asimov D., Globus A., Levit C., *Tutorial #6 "Topology, Vector Fields, and Flows"*. Visualization'92, IEEE Computer Society, 1992.

0-7803-5897-X/99/\$10.00 Copyright 1999 IEEE

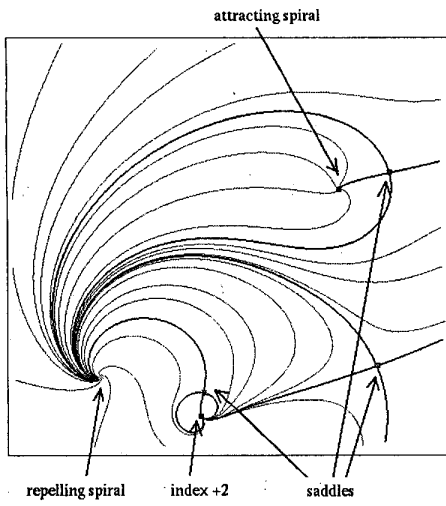


Figure 6: ex.1: topology of the original vector field

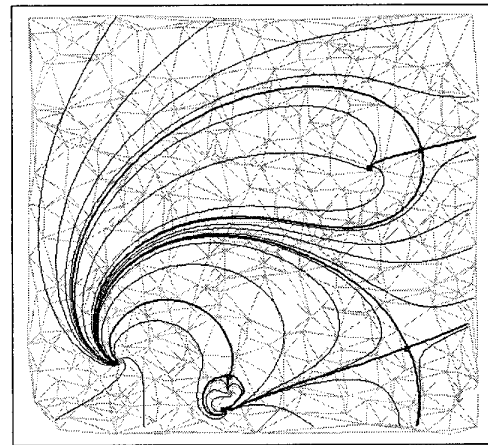


Figure 9: ex.1: Powell-Sabin method (500 samples)

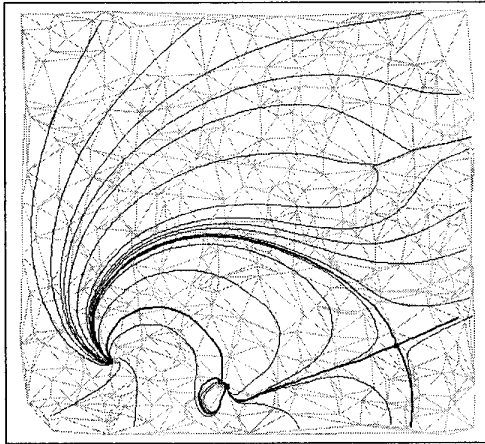


Figure 7: ex.1: linear interpolation (500 samples)

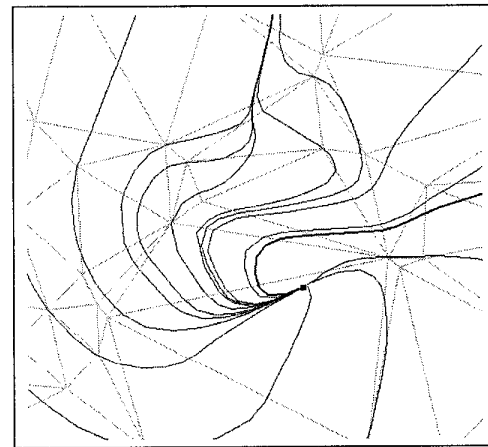


Figure 10: ex.1: linear interpolation around the higher order singularity (1000 samples)

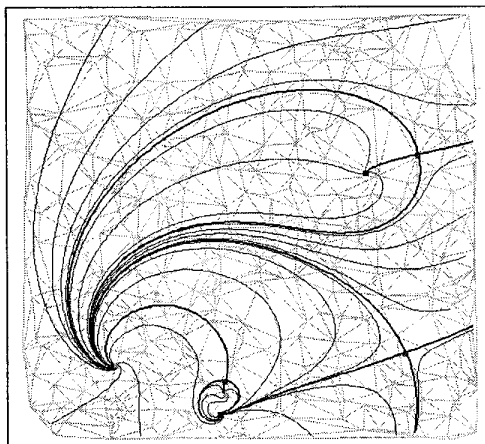


Figure 8: ex.1: Nielson's method (500 samples)

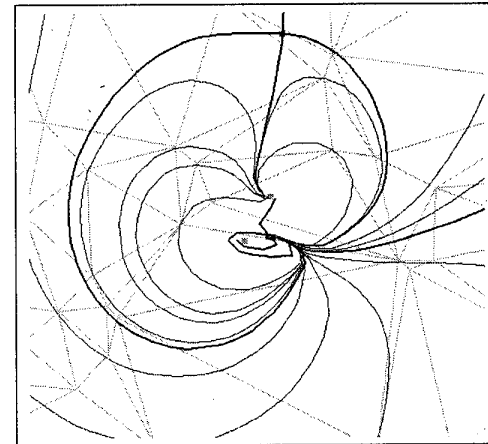


Figure 11: ex.1: Powell-Sabin method around the higher order singularity (1000 samples)

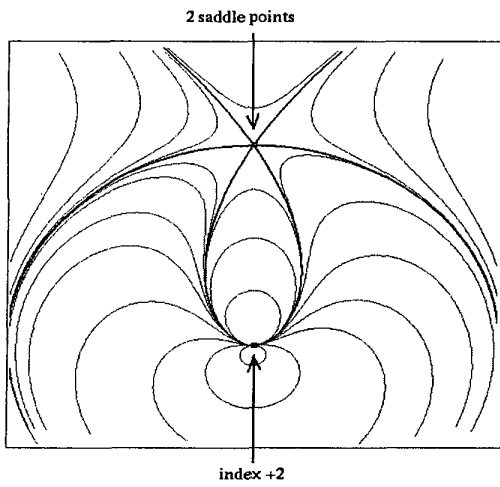


Figure 12: ex.2: topology of the original vector field

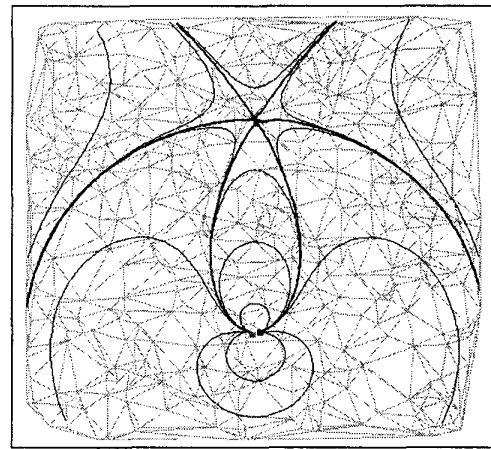


Figure 15: ex.2: Powell-Sabin method (500 samples)

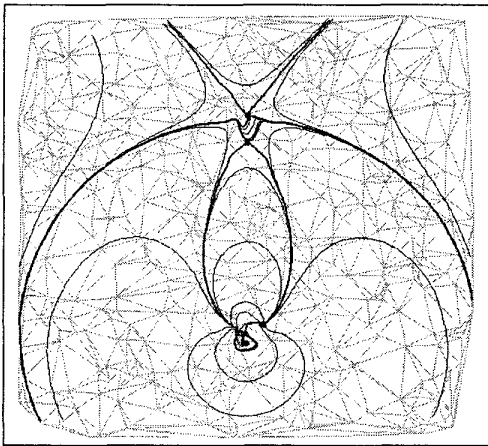


Figure 13: ex.2: linear interpolation (500 samples)

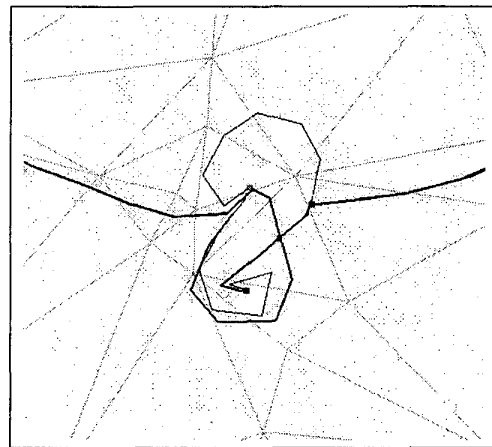


Figure 16: ex.2: linear interpolation around the higher order singularity (5000 samples)

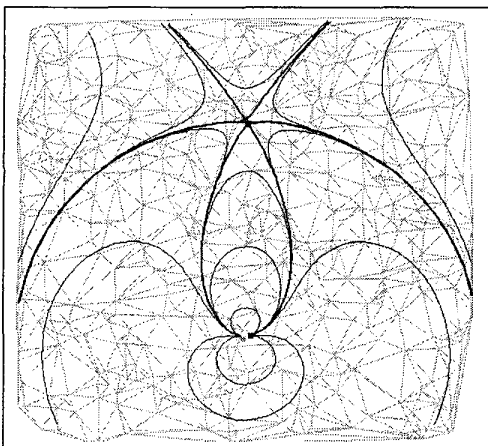


Figure 14: ex.2: Nielson's method (500 samples)

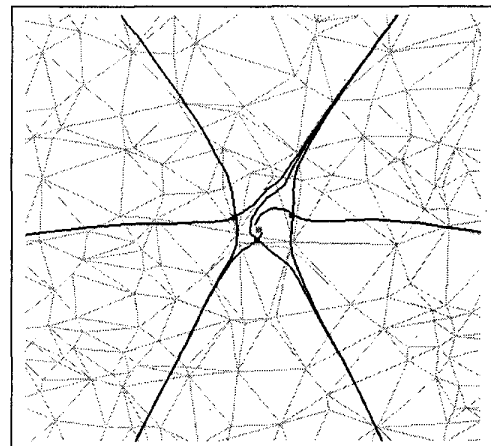
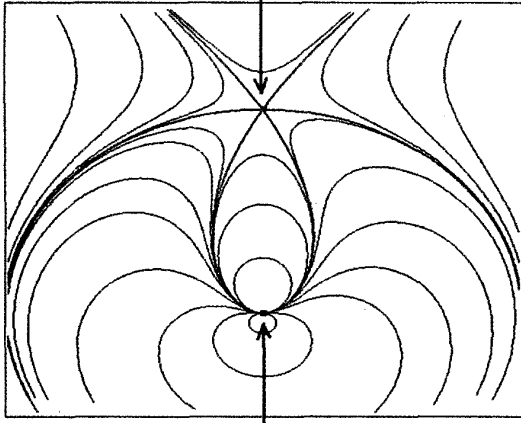


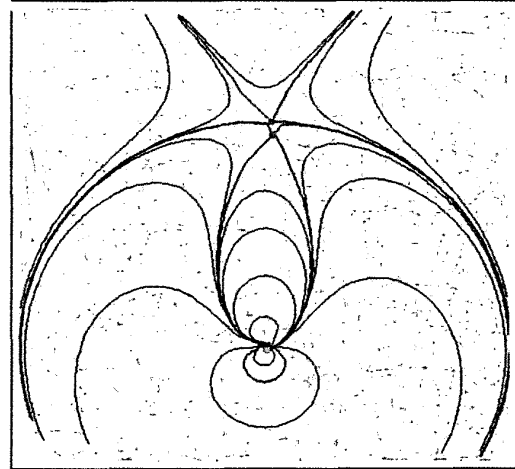
Figure 17: ex.2: linear interpolation around the two saddles (5000 samples)

2 saddle points

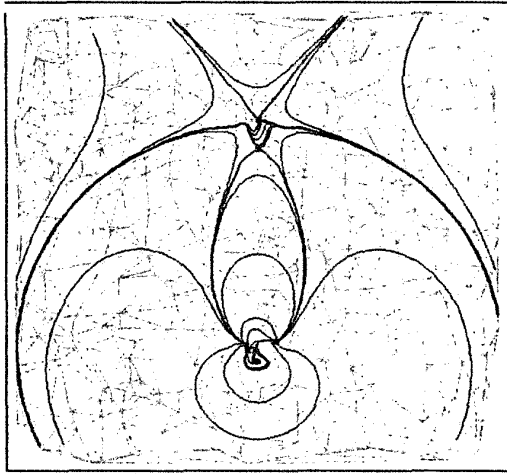


index +2

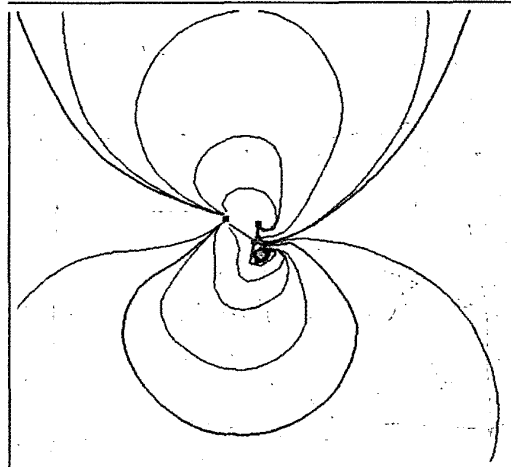
ex.2: topology of the original vector field



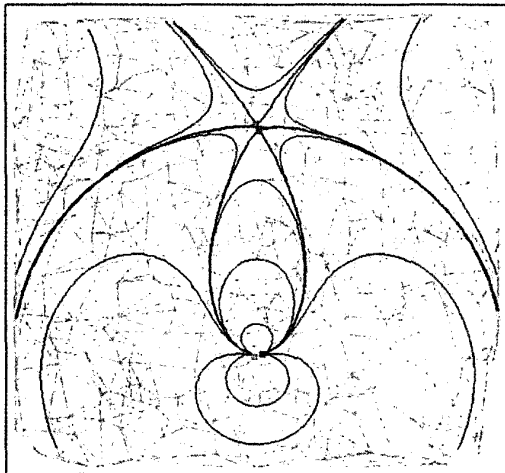
ex.2: linear interpolation (1000 samples)



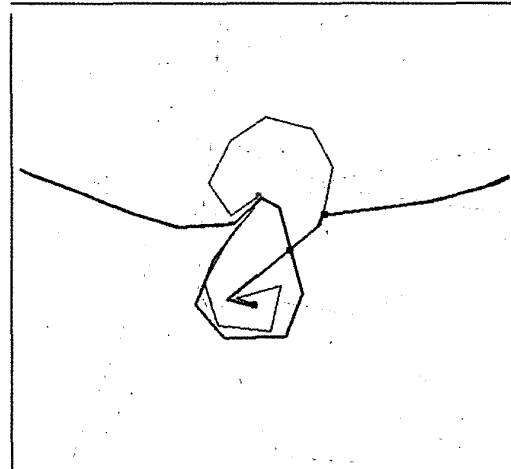
ex.2: linear interpolation (500 samples)



ex.2: linear interpolation around the higher order singularity (1000 samples)



ex.2: Nielson's method (500 samples)



ex.2: linear interpolation around the higher order singularity (5000 samples)

C1-Interpolation for Vector Field Topology Visualization
Gerek Scheuermann, Xavier Tricoche, Hans Hagen